INSTITUTE OF PHYSICS PUBLISHING JOURNAL OF PHYSICS: CONDENSED MATTER

J. Phys.: Condens. Matter **13** (2001) 6659–6674 PII: S0953-8984(01)24085-5

A rare-earth K-edge EXAFS study of rare-earth phosphate glasses, $(R_2O_3)_x(P_2O_5)_{1-x}$, x = 0.187–0.239, R = La, Nd, Sm, Eu, Gd, Dy, Er

Jacqueline M Cole[1,2,6], Robert J Newport[2], Daniel T Bowron[3], Robert F Pettifer[4], Gavin Mountjoy[2], Tessa Brennan[5] and George A Saunders[5]

[1] Department of Chemistry, University of Cambridge, Lensfield Road, Cambridge CB2 1EW, UK
[2] School of Physical Sciences, University of Kent at Canterbury, Canterbury, Kent CT2 7NR, UK
[3] European Synchrotron Radiation Facility, BP 220, F-38043 Grenoble Cedex, France
[4] Department of Physics, University of Warwick, Coventry CV4 7AL, UK
[5] Department of Physics, University of Bath, Claverton Down, Bath BA2 7AY, UK

E-mail: jmc61@cam.ac.uk

Received 19 April 2001, in final form 11 June 2001
Published 19 July 2001
Online at stacks.iop.org/JPhysCM/13/6659

Abstract

A rare-earth K-edge extended x-ray absorption fine structure (EXAFS) study of rare-earth phosphate glasses, $(R_2O_3)_x(P_2O_5)_{1-x}$, x = 0.187–0.239, R = La, Nd, Sm, Eu, Gd, Dy, Er, is presented. The structures of these materials were investigated as a function of (a) rare-earth atomic number and (b) temperature, and represent some of the first rare-earth K-edge EXAFS studies on a series of lanthanide-based materials. Results corroborate findings from complementary x-ray and neutron diffraction and magic-angle-spinning (MAS) NMR experiments, and in addition, they provide a unique insight into the nature of the static disorder of the R–O correlations and of the neighbouring phosphate groups. The effects of multiple-scattering contributions are also discussed within this context. The variable temperature measurements illustrate the exceptionally high level of network rigidity present in these materials. The results are also compared to those obtained from an analogous rare-earth L_{III}-edge EXAFS (5.483–8.358 keV) study. Results show that the use of the much higher energies of the rare-earth K-edge (38.925–57.486 keV) enable one to avoid the double-electron excitation problems that are associated with the rare-earth L_{III}-edge EXAFS in the dynamic range of interest. EXAFS fitting and deconvolution simulations show that the large core hole lifetimes associated with the rare-earth K-edge do not significantly detract from the results. The deconvolution studies also corroborate our findings that the level of fitting to our data cannot realistically be expanded beyond the first R–O shell. This limitation

[6] Author for correspondence. Present address: Department of Chemistry, University of Cambridge, Lensfield Road, Cambridge CB2 1EW, UK.

exists despite the exceptional counting statistics of the experiment and the highly uniform samples made possible by the ability to use much thicker samples at the higher energies compared to those used for the (higher absorption) rare-earth L_{III}-edge EXAFS studies.

1. Introduction

Rare-earth (R) phosphate glasses with stoichiometries close to those of metaphosphate, $R(PO_3)_3$, and ultraphosphate, RP_5O_{14}, species have shown great promise in the laser and optoelectronics industry. This is because the rare-earth ions possess the required energy levels for achieving successful population inversion and the non-linear refractive index is large enough to exhibit the desired optical effects without causing beam breakup and damage. Moreover, the particularly high concentration of rare-earth dopant present in these materials results in a myriad of exotic physical properties at low temperatures: negative thermal expansion (Acet *et al* 1998), negative pressure dependence of bulk moduli (Mierzejewski *et al* 1988) and unprecedented magnetic, magneto-optical and opto-acoustic phenomena (Carini *et al* 1997).

Despite this multitude of exciting properties, their fundamental structural origins are not well understood. The nature of the atomic structure of these glasses evidently plays an important role in their physical characteristics. However, such knowledge is sparse, to the extent that a concerted structural programme is being followed in order to establish a coherent picture of the glass microstructure.

Due to the high structural complexity of glasses, extensive use of a wide range of structural probes is necessary in order to piece together the structure of these materials. Previous work has concentrated on fluorescence (Farok *et al* 1992, Acet *et al* 1998, Brennan *et al* 1999) and Raman spectroscopy (Mierzejewski *et al* 1988, Lipinska-Kalita *et al* 1995), rare-earth L_{III}-edge EXAFS (Bowron *et al* 1995, 1996b, Anderson *et al* 1999) and x-ray absorption near-edge structure (XANES) (Mountjoy *et al* 2001), neutron (Hoppe *et al* 1998, Cole *et al* 1999) and x-ray diffraction (Bowron *et al* 1995, 1996a, Cole *et al* 2001), and MAS NMR (Cole *et al* 1999, 2001) techniques. The spectroscopic results showed that the rare-earth dopants exist as tripositive ions that are embedded in a phosphate network. Rare-earth L_{III}-edge EXAFS studies confirmed these findings and also yielded average R–O distances of 2.42(1)–2.23(1) Å (where R = La–Er), decreasing in accordance with the lanthanide contraction. In addition, the EXAFS results showed that the R^{3+} ions are surrounded exclusively by between six and eight oxygen ions, these limits corresponding to the coordination numbers of the ultra- ($x = 0.167$) and meta- ($x = 0.25$) phosphate crystalline analogues (see for example Cole *et al* 2000, Hong 1974). The EXAFS spectra also intimated the existence of a second neighbour R–(O)–P correlation in the vicinity of 3.1–3.6 Å and a third neighbour correlation, R–(OP)–O, in the region of 4.0–4.1 Å.

Complementary neutron diffraction studies (Hoppe *et al* 1998, Cole *et al* 1999) corroborated these EXAFS results and quantified the immediate rare-earth environment more precisely. Correlations due to the phosphate network were located and quantified; in particular, terminal and bridging P–O correlations were resolved well and second (O–(P)–O and P–(O)–P) and third (P–(OP)–O) neighbour separations were characterized. Aluminium impurities, incorporated within the glass network during sample fabrication, were also detected and their important role in strengthening these glass structures was deduced by ^{27}Al multi-quantum (MQ) MAS NMR investigations (Cole *et al* 1999).

The effects of aluminium in terms of rare-earth clustering were analysed via x-ray diffraction, and all pairwise atomic correlations were parametrized quantitatively out to a radial distribution of 4 Å. Through this procedure, details of the R–(O)–P and R–(OP)–O correlations were revealed for the first time. Together with ^{31}P MAS NMR measurements (Cole *et al* 2001), the x-ray diffraction work also helped in understanding the changing nature of the phosphate network as a function of rare earth concentration. The immediate R–O environment, however, appears to be invariant with changing composition, as deduced by rare-earth L_{III}-edge EXAFS and XANES studies, over the range of compositions between ultra- and metaphosphate (Mountjoy *et al* 2001).

It is therefore pertinent to quantify the level of static disorder in the vicinity of the R^{3+} ions. The rare-earth coordination number is important in this regard since the level of static disorder in the phosphate network is expected to vary as the R–O coordination number, N_{RO}, varies in the order $N_{RO} = 6 \rightarrow 8 \rightarrow 7$, owing to the decreasing packing efficiency about the R^{3+} ion. Given the fact that EXAFS is, relatively, a poorly conditioned probe of coordination numbers due to the difficulties of defining accurate absolute peak areas in the interference function, we here deduce N_{RO}, as a function of R^{3+} atomic number, indirectly from the rare-earth interatomic separations (R_{RO}): the R_{RO} values deduced from experiment are compared with R–O distances expected for a given coordination number, which are calculated from theoretical values of rare-earth ionic radii (Shannon 1976). The results are combined with those from previous complementary atomic probes, and a correlation between N_{RO} and the level of static disorder is derived.

The present study was also carried out in an attempt to determine the nearest-neighbour R...R interatomic distance, since (i) EXAFS data yield chemically specific pairwise atomic correlations, in contrast to conventional diffraction measurements, and so are affected less by overlapping peaks. Thus, one has the potential to identify the origins of correlation peaks at larger pairwise separations than diffraction results (which show that is no evidence of R...R correlations at distances of less than 4 Å); (ii) the use of the K-edge rather than the L_{III} edge provides a wider dynamic range in reciprocal space, and thus greater real-space resolution ($\Delta r \approx \pi / k_{max}$; in these studies the maximum scattering vector, $k_{max} \sim 16$ Å^{-1}). This derives from the facts that there are no higher energy absorption edges imposing a maximum limit on the available dynamic range, and the higher energies involved give a higher ratio of the cross-section of the rare-earth ion relative to the matrix. This provides a better signal to noise ratio, which in turn permits structure to be seen above the noise over a wider range of k. The use of low measurement temperatures minimizes the thermal disorder, thereby reducing further the severity of damping effects.

Knowledge of the closest R...R approach in these materials is pertinent since it has direct consequences on the observed physical properties: too close a separation severely impairs the optical and magnetic properties of these glasses. The measurement of EXAFS spectra as a function of temperature (values of $T = 20$ K, 50 K and 80 K were studied) was also important in order to assess whether or not, within the limitations of EXAFS as a probe method, the unusual physical properties observed below $T \sim 20$ K emanate from structural origins.

In addition to the direct structural information on the subject materials that can be gleaned from this study, this work also represents one of the first rare-earth K-edge EXAFS studies on a *series* of amorphous materials, each containing a different rare-earth ion: whilst there exist several reports of other rare-earth K-edge EXAFS studies (e.g. Borowski *et al* 1999, Braglia *et al* 1998, 1999a, b, Kasatani *et al* 1999), owing to the high energies now becoming commonly accessible via 'third generation' synchrotron x-ray sources, previous work has concentrated on probing single particular rare-earth containing species. Furthermore, to our knowledge, this work represents the first report of a rare-earth K-edge EXAFS study, probing rare-earths of

greater atomic number than Eu, that yields quantitative structural information. This absence of published data arises in part from the effect of core hole lifetime broadening as a function of rare-earth atomic number. The data presented herein therefore also provide a valuable insight into the level of information that can be drawn from such a study, despite the problems associated with and arising from the core hole lifetime broadening, which are deemed to be significantly adverse in previous literature on rare-earth K-edge EXAFS (e.g. Nishihata *et al* 1998).

2. Experiment

2.1. Sample preparation and characterization

All glass samples were prepared by heating 25 mol% of the high purity (99.9%) grade rare-earth oxide in the presence of excess P_2O_5 in an aluminium oxide crucible at a temperature corresponding to the rare-earth oxide melt (1400–1650 °C); full synthetic details are described by Mierzejewski *et al* (1988). The challenging thermal conditions of the synthetic process make it difficult, to some degree, to attain exact compositional precision. However, it is possible to synthesize such materials within the compositional region of meta- and ultraphosphate. The rare-earth concentrations in the resulting samples were deduced by electron probe microanalysis, and their atomic densities were measured by conventional gravimetric analysis. The crystalline NdP_5O_{14} sample, used as a standard reference material, was prepared according to the procedure of Danielmeyer *et al* (1974).

2.2. K-edge EXAFS experiments

All experiments were carried out on the bending magnet x-ray absorption spectroscopy beamline, BM29, at the European Synchrotron Radiation Facility (ESRF), Grenoble, France. The synchrotron storage ring was operating at 6 GeV in two-thirds fill mode, yielding typical currents of 150–200 mA. A Si(511) double crystal monochromator, detuned by 50% for harmonic rejection, was used throughout the experiment, providing a flux at the sample position of $\sim 10^8$ photons s^{-1}. Primary vertical slits of 0.3 mm provide an energy resolution of 5 eV, which is less than one-third of the core hole lifetime broadening expected from the rare-earth K-edges (16–29 eV (La–Er)). All data were collected using standard transmission geometry and ion chamber detectors. The monochromator was calibrated using a Gd foil adopting 50.239 keV as the energy of the inflection point of the edge.

The finely powdered glass samples were diluted in a uniform manner by mixing them into a polyethene matrix (in a 1:1 ratio by volume) and pressing them into a pellet of a thickness $\sim$3 mm. The low level of x-ray absorption at the high energies used for the experiment (38.925–57.486 keV) permit this substantial sample thickness, which is highly advantageous in terms of achieving good uniformity in optical thickness, in contrast to those required for analogous L_{III}-edge EXAFS experiments. Samples were placed in an Oxford Instruments closed-cycle refrigerator based helium cryostat and measured at three different temperatures, $T = 20$ K, 50 K and 80 K. In addition, spectra were also collected for the gadolinium sample at 145 and 293 K.

The EXAFS spectra were recorded using a pre-edge energy range of at least 225 eV and a post-edge energy range corresponding to $k_{max} = 19.6$–28.4 Å^{-1}, using a wavevector scanning increment above the edge, $\Delta k = 0.05$–0.02 Å^{-1}, and with a minimum edge step of 0.8. In the majority of cases the maximum value of k was chosen on the basis of the extent to which there remained significant structure in the data in k-space. Spectra were collected in multiple scans and averaged, using a total integration time of 6–10 s/point and yielding a corresponding signal-to-noise ratio of $\sim 10^4$.

The transmitted x-ray intensity data, $I_t(k)$, were averaged and normalized to the incident x-ray beam, I_0, and background corrections were performed using EXBACK (Binsted *et al* 1991). The normalized absorbance function, $\chi(E) = (\mu t(E) - \mu t_{pre})/(\mu t_{post} - \mu t_{pre})$, in which the absorption function, minus the extrapolated pre-edge absorption and normalized by the edge step, was modelled in EXCURV92 (Binsted *et al* 1991) according to fast curve-wave theory (Pettifer and Cox 1982, Mustre de Leon *et al* 1991, Gurman *et al* 1984, 1986):

$$\chi_l(k) = -\sum_j N_j S_0^2 \frac{|f_{eff}(\pi, k, R)|}{kR^2} \sin(2kR + 2\delta^c + \phi_{eff})\, e^{-2\sigma^2 k^2}\, e^{-2R/\lambda}$$

where k is the wavevector of the photoelectron, R is the nearest-neighbour distance, N_j is the coordination number, $2\sigma^2$ is the Debye–Waller term, which describes the level of static and dynamic disorder, $f_{eff}(\pi, k, R) = |f_{eff}(\pi, k, R)|e^{i\Phi_{eff}}$ is the effective curved-wave backscattering amplitude, δ^c is the final-state l-wave central atom phase shift, λ is the mean free path of the photoelectron for inelastic scattering and S_0^2 describes the amplitude reduction owing to many-body effects (Li *et al* 1995, Mustre de Leon *et al* 1991). In this heuristic equation, R, N_j and $2\sigma^2$ are refinable parameters whereas the other variables are derived from atomic potential calculations (Li *et al* 1995). In terms of calculating the ground-state potentials and the ground-state exchange energy of the excited photoelectron, von Barth and Hedin–Lundqvist potentials were utilized for this study respectively (Li *et al* 1995) and the $Z + 1$ approximation was used to take account of the core hole relaxation (Stern and Kim 1981). EXAFS data of an NdP_5O_{14} polycrystalline material were collected under the same experimental conditions as the glasses, and the data analysed such that the parameters relating to the many-body amplitude reduction effects were refined whilst the R, N_j and $2\sigma^2$ parameters were constrained to known values[7].

A model of the local environment of the R^{3+} ion was refined against the data by a least-squares process, starting from initial R, N and $2\sigma^2$ parameters for each shell modelled. Estimated standard deviations for each of these parameters were taken from the contours, at the 2σ level, in correlation maps of the appropriate pairs of variables: R versus E_F (the Fermi energy parameter, which is also refined from the data) and N versus $2\sigma^2$. It should be borne in mind that such errors represent a minimum estimation since the statistical basis of their derivation ignores systematic effects such as those arising from multiple scattering, overlapping correlation shells, systematic instrumental errors or Fourier transform artefacts at low R. In the present case, the multiple scattering is shown to be small within the shell fitted. These errors are, however, a better guide to fitting uncertainties than the use of fitting algorithm statistical information alone.

2.3. *Multiple scattering calculations*

Curved-wave theory is essentially an extension of the plane-wave approximation (Sayers *et al* 1971), this being superceded since the approximation breaks down at low k (Lee and Pendry 1975). However, the implementation of curved-wave theory, in codes such as EXCURV, is intrinsically limited by the fact that it is difficult to incorporate reliably multiple scattering pathways into the fitting procedure. A single scattering assumption is reasonable for large values of k, but for values up to $k \sim 7$ Å^{-1}, significant multiple scattering effects (up to 10% of single scattering) have been observed in a variety of structures (Zabinsky *et al* 1995, Kuzmin

[7] Such values were derived from an in-house single crystal diffraction structure determination of NdP_5O_{14}, since the published structure was carried out at room temperature and gave nonsensical non-positive definite anisotropic displacement parameters, owing to the greater experimental limitations at the time of the publication compared to those available now.

and Grisenti 1994). Such effects are most prevalent in data where the local environment of the central atom has a certain level of local symmetry such that the scattering pathways allow constructive interference over many similar conformations in the structure. Given the suggested average six- to sevenfold coordination level of oxygens surrounding the rare earths in these glasses (Cole *et al* 1999, 2001) and basic energy stabilization considerations, local symmetries resembling distorted octahedral, capped octahedral or pentagonal bipyramidal environments were regarded as useful heuristic models. An estimate of the level of multiple scattering could therefore be ascertained prior to constructing and refining a model against the data presented here; in this case, the distorted octahedral local symmetry was considered the most realistic, cf analogous ultra- and metaphosphate crystalline geometries (Hong 1974, Cole *et al* 2000).

In order to assess the extent to which multiple scattering existed in these materials, the GNXAS suite of programs was utilized (Filipponi *et al* 1992, Di Cicco 1995, 1997). Here, the total scattering is calculated in terms of irreducible n-body distribution functions, $\gamma^{(n)}$ (Filipponi *et al* 1995, Filipponi and Di Cicco 1995), which are linear combinations of continued fractions (Filipponi 1991). The EXAFS $\chi(E)$ function is expanded in terms of $\gamma^{(n)}$ to represent the full contribution to the scattering. Such an expansion is used since it has a better convergence rate than that of an infinite formal multiple-scattering series calculation, i.e.

$$\sum_{n=1}^{\infty} \chi^n.$$

The values of $\gamma^{(n)}$ are calculated using a model of the environment surrounding the core central atom, the various single and multiple scattering pathways containing n atoms (atoms may be duplicated) being calculated within a radial limit. For each type of pathway, scattering contributions are binned into distance ranges according to a specified tolerance and the most intense groupings are assessed.

Given the difficulty of assigning unique multiple scattering pathways to an amorphous structure, and given the existence of relevant structural parameters derived from experimental data within our group (Cole *et al* 2000), the results from a model generated from the lanthanum ultraphosphate crystal structure were examined in order to provide useful insights into the glass analogues. This is an intrinsically 'artificial' exercise, but ought nevertheless to offer heuristic insight into the possible effects of multiple scattering pathways in the glass. In the calculations, muffin tin radii for each atom type were evaluated from the partitioning of bonds from the LaP_5O_{14} crystal structure. The best fitted partitioning scheme resembled very closely a wholly ionic model (Shannon 1976, Jia 1991) despite an ostensible covalent tendency envisaged within the phosphate network. The ionic radii used were $La^{3+} = 1.20$ Å, $P^{5+} = 0.17$ Å and $O^{2-} = 1.30$ Å.

2.4. Deconvolution studies

An inherent limitation of x-ray absorption spectroscopy of deep core holes is that associated with their lifetime broadening which, in the context of lanthanide K-edges may approach ~30 eV. However, where good data quality is available that has fully exploited the stability of new generation sources and monochromators, it has been demonstrated that lifetime broadening may partially be removed by a deconvolution process (Loeffen *et al* 1996). The procedure, which is justified with an error estimation from Shannon–Hartley information theory (see Shannon and Weaver 1963 or Young 1971), partially removes some of the lifetime broadening; in our case the core hole dominated K-edge width is reduced by 9.5 eV. A result of information theory is that by artificially increasing the band-width (reducing the lifetime) the noise level

is increased. Since the information content of the data before and after deconvolution is the same (the process is reversible), the technique is a representation of the data and serves to visibly enhance features that are already present and which are subject to the least-squares fitting procedures. The data presented herein were therefore suitable for such a study, the subject compounds being the La and Er glasses as these represent, respectively, the minimum and maximum lifetime broadening effects in this series.

3. Results

The compositions of each $(R_2O_3)_x(P_2O_5)_{1-x}$ glass studied are given in table 1. The k^3-weighted 20 K K-edge EXAFS spectra of all subject compounds are illustrated in figure 1; those from

Table 1. The fitted parameters for the first R–O shell environment of rare-earth phosphate glasses, $(R_2O_3)_x(P_2O_5)_{1-x}$. (The composition given does not take into account the fact that all samples are known to also contain 1–2 wt% of aluminium impurity).

R^{3+}	Comp.	R–O parameters 20 K			R–O parameters 50 K			R–O parameters 80 K		
ion	x	R (Å)	N	$2\sigma^2$ (Å^2)	R (Å)	N	$2\sigma^2$ (Å^2)	R (Å)	N	$2\sigma^2$ (Å^2)
La	0.225	2.434(9)	8.0(8)	0.016(3)	2.432(8)	7.9(8)	0.016(2)	2.427(11)	8.4(9)	0.018(2)
Nd	0.187	2.367(9)	7.6(9)	0.013(2)	2.366(6)	7.6(7)	0.013(2)	2.369(7)	7(1)	0.013(2)
Sm	0.226	2.321(9)	7(1)	0.011(2)	2.321(7)	6.8(5)	0.013(2)	2.316(9)	6.9(7)	0.012(2)
Eu	0.208	2.330(9)	6.1(6)	0.011(2)	2.336(6)	6.7(6)	0.011(2)	2.329(4)	6.5(8)	0.011(2)
Gd[a]	0.229	2.301(9)	8(1)	0.012(3)	2.304(7)	7.0(8)	0.011(2)	2.303(9)	7.0(8)	0.012(3)
Dy	0.225	2.265(6)	5.9(5)	0.011(2)	2.274(7)	5.7(6)	0.011(2)	2.270(7)	5.7(7)	0.012(2)
Er	0.239	2.236(6)	6.4(8)	0.010(2)	2.235(7)	6.7(7)	0.011(2)	2.234(7)	6.3(7)	0.009(2)

[a] Additional R, N and $2\sigma^2$ parameters for the 145 and 293 K $(Gd_2O_3)_{0.229}(P_2O_5)_{0.771}$ data-sets are respectively: 2.307(7) Å, 6.9(7), 0.012(2) Å^2 and 2.302(7) Å, 6.7(7), 0.013(3) Å^2.

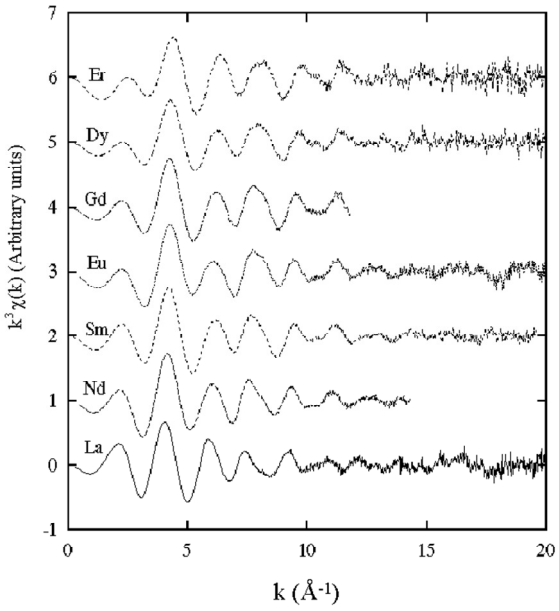

Figure 1. The experimental 20 K K-edge EXAFS spectra of the rare-earth phosphate glasses studied.

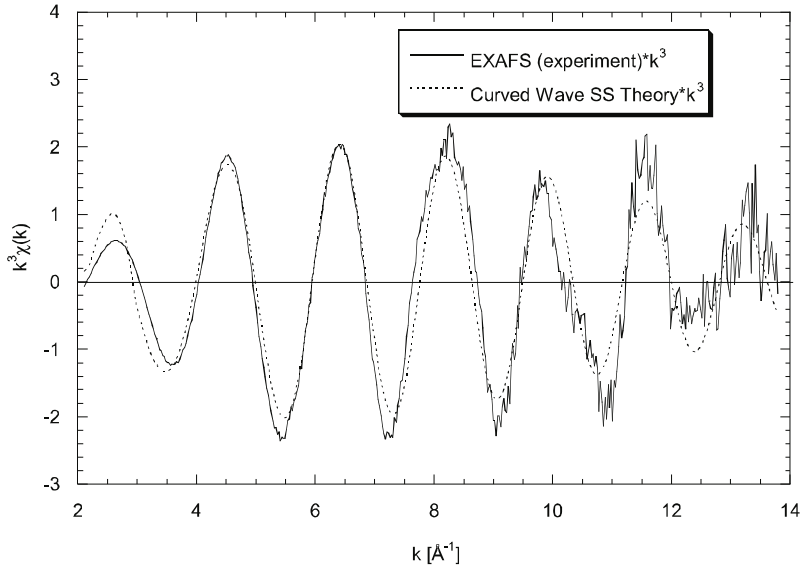

(a)

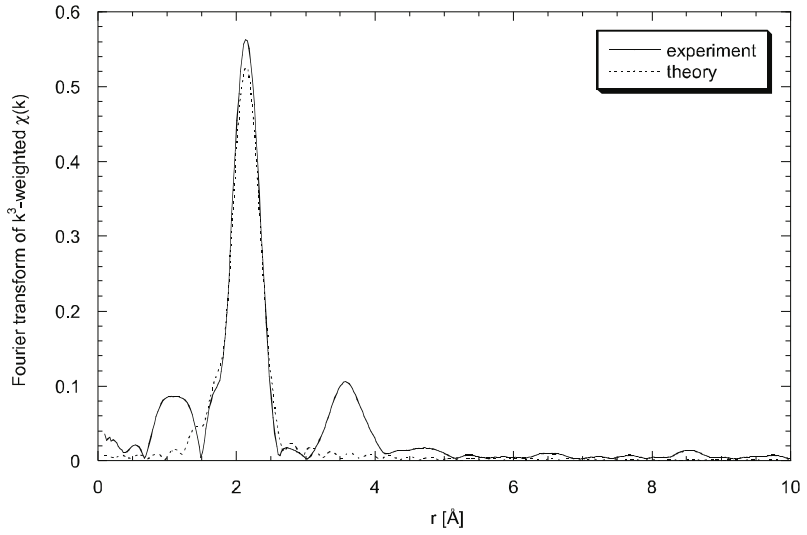

(b)

Figure 2. Example plots using the data from $(Er_2O_3)_{0.239}(P_2O_5)_{0.761}$: (a) k^3-weighted $\chi(k)$ of the 20 K K-edge EXAFS data, together with the corresponding EXCURV92 fit; (b) the Fourier transform of the k^3-weighted $\chi(k)$ as a function of distance (Å). The parameters of the fit are given in table 1.

data collections at 50 and 80 K appear very similar. Figure 2 exemplifies the $k^3\chi(k)$ fit to the data and corresponding Fourier transform features that typify these spectra, using the 20 K erbium data as the example. Figure 3 shows the Fourier transform features for all data sets at 20 K; those deduced from measurements made at all other temperatures are very similar. The exceptionally good quality of the data is evident, particularly in the range $k < 12$ Å^{-1}, and the range over which significant oscillations are discernible extends, in some cases, to

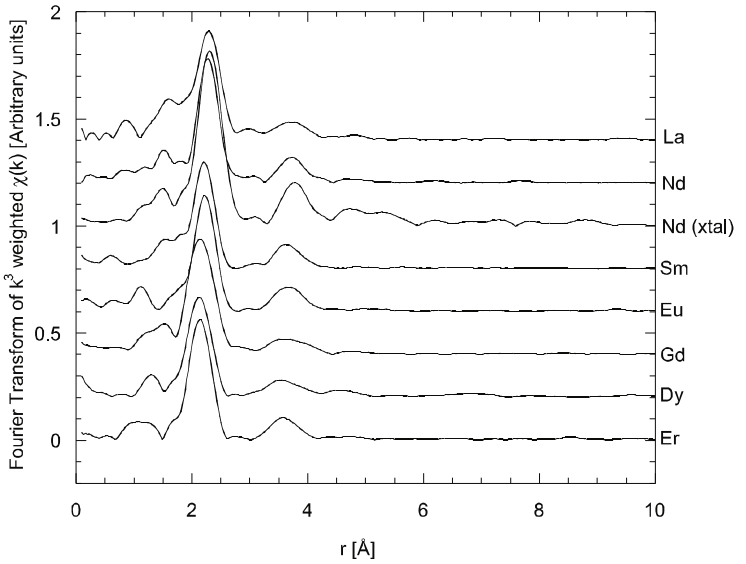

Figure 3. The Fourier transform of the k^3-weighted $\chi(k)$ as a function of distance (Å) for all data sets of glasses collected at 20 K and for the crystalline standard, NdP_5O_{14}. The effects of the lanthanide contraction can be seen by the progressive shortening of the first neighbourhood as a function of rare-earth atomic number. The broader features present in the farther neighbourhoods are also evident and a comparison of the crystalline NdP_5O_{14} versus $(Nd_2O_3)_{0.187}(P_2O_5)_{0.813}$ glass structure is made.

$k \sim 26$ Å^{-1}. The relative magnitudes and phases of the spectra vary with R^{3+} but the generic features are common to all.

The model of the total EXAFS scattering contributions in crystalline LaP_5O_{14} is given in figure 4. The simulated data shown in figure 4 shows broad similarities with the experimental data of figure 1, which suggests that our ultraphosphate model exhibits structural attributes that may be regarded as reflective of the structure of the glass. In this context, we note immediately that the single-scattering [$\gamma^{(2)}$] effects arising from pairwise correlations at ~2.5 Å, i.e. owing to R–O, dominate the total EXAFS signal and significant structure is present up to at least 15 Å^{-1}.

Similarly, we observe that single scattering beyond the first shell is weak, contributions being substantial only up to $k \sim 6$ Å^{-1}, and all resulting from scattering pathways between atoms with interatomic distances $\geqslant$4 Å. Indeed, figure 4 shows only the strongest terms derived from our simulation, all other pairwise terms being even weaker. This is of significance since, on the basis of simple geometrical arguments, the nearest-neighbour distance, R...P, must lie below this lower bound. Moreover, previous x-ray diffraction studies on these materials (Cole *et al* 2001) have shown that this correlation actually exists at ~3.7 Å. The backscattering from the neighbouring phosphorus must therefore be attenuated in some way, or occluded by multiple scattering or by single scattering from the second R...O coordination sphere (which encase the phosphorus environment). Given the proximity of P and O in the periodic table, it is difficult to make definitive assignments at this level other than to note that there exist many more oxygens than phosphorus at this radial distance from R^{3+} and the ionic size of P^{5+} is much smaller than that of the O^{2-} ion.

The closest R...R approach in LaP_5O_{14} lies at 5.246 Å (Cole *et al* 2000) and so, given the lack of apparent backscattering from phosphorus, the single scattering effects emanating from

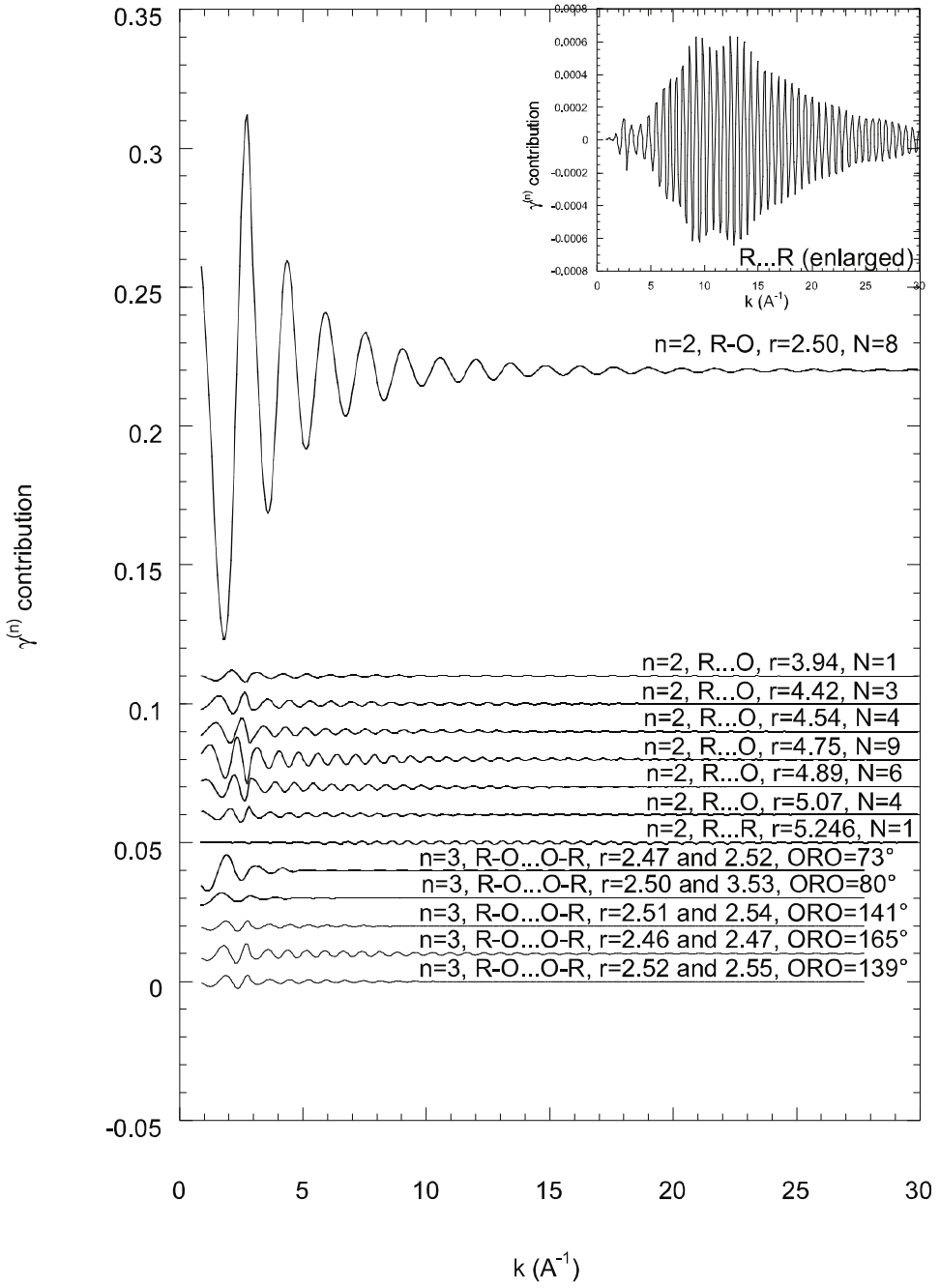

Figure 4. The simulated irreducible n-body $\gamma^{(n)}$ contributions to the EXAFS signal for crystalline LaP_5O_{14} as a function of the scattering vector, k. The pairwise R...X interatomic distances, r, and $O\hat{R}O$ angles of each correlation were taken from the LaP_5O_{14} crystal structure (Cole *et al* 2000). Where multiple correlations, of a given type, are present in close proximity to each other (0.1 Å tolerance), the N contributions were grouped together. An enlargement of the $\gamma^{(n)}$ contribution from the R...R correlation comprises the inset.

pathways in the range ~3.3–5.0 Å must presumably be due to R...O correlations exclusively. The model depicts six discrete sub-shells within this range, but the spread of these shells suggests that their effective contribution in r-space will be unresolvable from one another. Indeed, in the Fourier transform of the crystalline NdP_5O_{14} experimental data (see figure 3), one observes several unresolved features in exactly this range. In the glasses data, only one very broad distribution can be resolved. This implies a significantly greater level of static disorder in the glasses, as one would expect.

The EXAFS contribution arising from the closest R...R separation appears to be small given its simulated characteristics (see figure 4). However, its most prominent effect on the spectrum appears at fairly high values of $k \sim 9$–15 Å^{-1} (see inset of figure 4) thus implying possible significance at frequencies that correspond to low values of r in real space. All attempts to fit this shell failed, however, owing to the omnipresence of obscuring secondary R...O scattering contributions that affect the real space function in this vicinity.

Multiple scattering effects are predicted in addition to single-scattering events, and significant effects derive from pathways encompassing three atoms ($\gamma^{(3)}$ contributions). Such effects appear significant only up to $k \sim 4$ Å^{-1} and will therefore induce relatively long-range features in real space. There are two types of multiple scattering contribution concerned here: both derive from R–O...O–R pathways, one where the O$\hat{\text{R}}$O angle lies at 70–80° (for $\gamma^{(3)}_{1-2}$), thus resembling a 'triangular' formation, whilst the other has an O$\hat{\text{R}}$O angle within the more 'linear' range 140–165° ($\gamma^{(3)}_{3-5}$). The convolution of their associated interference functions with one another and with the single-scattering event may be a cause of the additional diffuse signal in real space at distances in the realm of the broad second R...O coordination sphere discussed above. Such effects therefore hinder any attempt to formulate a quantitative assessment of structural information beyond the first shell. Indeed, all attempts to fit the experimental data beyond the immediate R–O environment failed due to the combination of the multiple-scattering effects, the very broad second R...O coordination sphere and the lack of intensity to the phosphorus backscattering.

The results of our lifetime broadening deconvolution studies are shown for the erbium data in figure 5, which represents the data most affected by the lifetime broadening effects. Here, there is no clear evidence for multiple-scattering contributions at low values of k. However, the results show clearly a deviation from sinusoidal behaviour at about 250 eV from the edge, indicating that the data contain information from more than one shell. This is in agreement with figure 2, which shows clearly the contribution from a second shell or group of shells centred between 3 and 4 Å in the Fourier transform.

In the corresponding deconvolution study of the lanthanum glass (representing the minimum lifetime broadening effects in this series) there is some evidence of a shoulder on the high energy side of the leading peak and of an asymmetry to the first EXAFS peak, but these have no direct impact on the conclusions we draw below. This additional structure may be of benefit to a full multiple-scattering investigation, but this is beyond the scope of the present paper. Here, however, the residual of the deconvolution fit shows that systematic errors are significant (possibly associated with the monochromator control algorithm used within the context of the non-uniform angular step sizes employed in the EXAFS scanning setup).

Given what has been established above regarding the limitations we feel must be applied to the data interpretation, the fact that our data could not be modelled sensibly beyond the first shell is understandable. However, the deconvolution studies do illustrate that the fitting of the first-shell information is reliable and has not utilized spurious features in the EXAFS spectra. The accurate modelling of the first R–O coordination shell (made feasible by the excellent counting statistics and the fact that the experimental data presented herein are largely

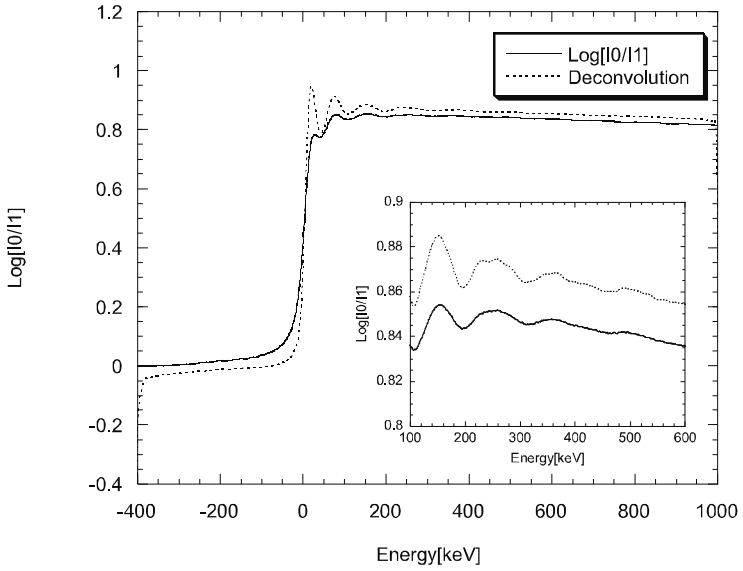

Figure 5. The results of the deconvolution studies for the Er K-edge EXAFS spectra of $(Er_2O_3)_{0.239}(P_2O_5)_{0.761}$. Solid and dashed lines represent the non-deconvoluted and deconvoluted experimental data respectively.

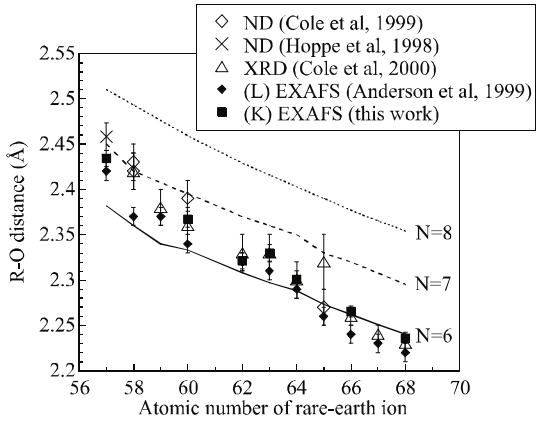

Figure 6. The variation of the nearest-neighbour R–O distance as a function of rare-earth atomic number, R, according to neutron diffraction (ND; Cole *et al* 1999, Hoppe *et al* 1998), x-ray diffraction (XRD; Cole *et al* 2001), K-edge EXAFS (this work) and L_{III}-edge EXAFS (Anderson *et al* 1999) studies. The lines on the plot represent the variation in R–O distance expected from tabulated values of calculated ionic radii for R^{3+} (Shannon 1976).

devoid of double-electron excitation effects, up to at least $k = 12$ Å^{-1}) is extremely valuable in and of itself. This contrasts with previous L_{III}-edge EXAFS measurements on these samples (Anderson *et al* 1999) where analysis was hindered by both data quality and double-electron excitation effects, the latter being particularly serious for the samples containing rare earths early in the lanthanide series.

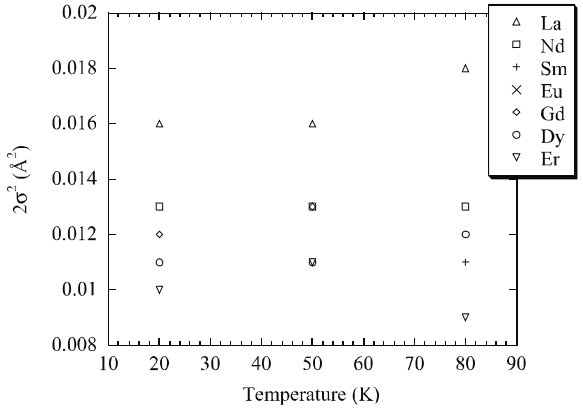

Figure 7. The K-edge EXAFS derived Debye–Waller factors, $2\sigma^2$, of the rare-earth phosphate glasses presented as a function of temperature. The estimated errors associated with each point are ±0.002–0.003.

The R–O shell was fitted using experimental data up to k_{max} = 11–16 Å^{-1} (this corresponds to a k_{max} = 22–32 Å^{-1} in conventional diffraction terms, which is larger than that useable in our previous conventional x-ray diffraction studies (Cole *et al* 2001). The parametrization of each R–O correlation is summarized in table 1 and the dependence of the refined parameters as a function of rare-earth atomic number is illustrated in figures 6 and 7.

4. Discussion

The R_{RO} values derived from this study compare very well to complementary results from previous diffraction studies (Cole *et al* 1999, 2001, Hoppe *et al* 1998) and adhere to the effects of the lanthanide contraction, as expected. The values are consistently larger, and determined with greater precision than those derived from the analogous L_{III}-edge EXAFS study (Anderson *et al* 1999). Indeed, the improved agreement of the present results with diffraction data indicates that a systematic error may have affected the L_{III}-edge EXAFS results, as was suggested by Anderson *et al* (1999). Given the relatively large fractional errors for the N_{RO} parameters, the R_{RO} values were used, in conjunction with tabulated values of ionic radii (Shannon 1976), to ascertain the trend in N_{RO} as a function of R^{3+} atomic number. The results confirm the apparent trend of increasing N_{RO} as the size of the R^{3+} ion increases, N_{RO} rising from 6 to 7 notably in the glasses where R = La to Nd.

Figure 7 illustrates that the Debye–Waller term decreases as the R^{3+} atomic number increases, and that this is the case irrespective of temperature, within the range T = 20–80 K. Only the samarium data fall slightly out of line with the otherwise consistent trend; however, the difference between values for the gadolinium and samarium data are only marginally significant, and given the wholly statistical origin of the quoted errors, the trend observed may be considered to be consistent over all R^{3+} ions studied. For each glass, all Debye–Waller values are the same, within experimental error, for the measurements at 20 K, 50 K and 80 K, and for the gadolinium glass, at least, the Debye–Waller factor appears invariant over the larger temperature range, 20–145 K. Therefore, not only may we conclude that the dominant contributing factor to the Debye–Waller values must be static disorder (i.e. as opposed to

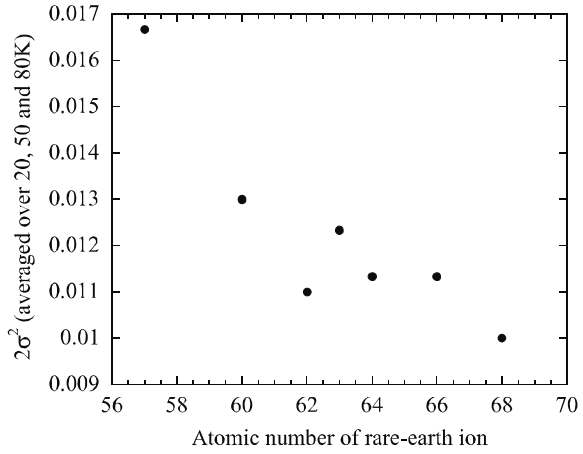

Figure 8. The averaged (over 20 K, 50 K and 80 K) Debye–Waller factors, $2\sigma^2$, of the rare-earth phosphate glasses presented as a function of rare-earth atomic number. The estimated errors associated with each point are ±0.002–0.003.

that induced by thermal motions[8]) but also that the data may reasonably be averaged across the various temperatures, and thereby provide improved statistical quality overall. Figure 8 illustrates the corresponding average $2\sigma^2$ values, presented as a function of R^{3+} atomic number, which emphasizes the observed trend even more clearly. A similar trend is tentatively apparent by the less well defined L_{III}-edge EXAFS results (Anderson *et al* 1999) measured in the temperature range, 80–293 K. No analogous trend may be observed in the diffraction results, owing to the obscuring effects of overlapping O(R)O correlations, which reduce the definition of the analogous $2\sigma^2$ values. The elucidation of this trend in the Debye–Waller values may be seen as congruent with the increase in N_{RO} associated with decreasing R^{3+} atomic number: the greater the values of the Debye–Waller term for the R–O correlation, the more static disorder is present, which in its turn reflects the nature of the decreasing packing efficiency of oxygens around the rare earth as N_{RO} changes from 6 to 7. In turn, the Debye–Waller values are also consistent with the lanthanide contraction as expected.

In absolute terms, the values of Debye–Waller factors are small which, given the invariance of temperature on these values, is consistent with the observation that the glasses are highly rigid. The hardness of these glasses has been alluded to before in the context of the importance of aluminium impurities within them (Cole *et al* 1999). Finally, one should record the obvious additional fact that no significant temperature effects pertaining to the anomalous physical properties of these materials at $T = 20$ K were observed.

5. Conclusions

The recent advances in synchrotron technology that enable rare-earth K-edge EXAFS experiments to be undertaken, yield data of very high quality which does not suffer from double-electron excitation features up to $k = 12$ Å^{-1}, in contrast to analogous L_{III}-edge EXAFS measurements. A much larger range of data can also be accessed since the k_{max}

[8] The Debye–Waller factor comprises both static and dynamic terms, which are combined in quadrature to obtain the resultant total, but the $2\sigma^2$ values are small and indifferent with temperature, within experimental error, and so the level of dynamic disorder is assumed to be constant relative to the static changes. We make the plausible assumption that the static disorder is greater than the effects of the zero point motion.

is not restricted by higher energy absorption edges. The low level of absorption at these higher energies also effects better sample uniformity since much thicker samples can be used. The K-edge EXAFS results confirm the trend of decreasing N_{RO} as a function of R^{3+} atomic number from 7 to 6, this change principally taking place between La and Nd. The results show clearly for the first time the presence of a concomitant decrease in static disorder, owing to the increasing packing efficiency around the rare-earth ion as it tends towards a six-coordinate rare-earth environment. The investigation over the temperature range 20–80(–293) K, also showed that the glasses are extremely rigid: the Debye–Waller factors of the R–O shell being very small and equal within experimental error.

The simulations on crystalline LaP_5O_{14} indicate that the nearest neighbour R–O shell dominates the EXAFS scattering and the contribution from the second R. . .O coordination shell is significant only up to $k \sim 6$ Å^{-1}. In addition, the R. . .O shell lies over a very broad range in real space, between ~3.3 and 5.1 Å. Multiple scattering affects the data up to $k \sim 4$ Å^{-1}, and complicate the spectra somewhat in this range, although theoretical calculations indicate that the magnitude of the effects are small compared with the principal single scattering pathways (within the limitations of the use of muffin-tin potentials). The disorder present in the glasses exacerbates the diffuse nature of these contributions and the R. . .O shell cannot satisfactorily be modelled. The resulting broad features in real space, similarly occlude the small scattering effects owing to the closest R. . .R separation.

Acknowledgments

The authors wish to thank R A Martin and H B Senin for the provision of the Sm and Eu samples respectively, the INFN, Italy, for the provision of the GNXAS software, and Dr Adriano Filipponi for advice on its use. We are grateful to the EPSRC for funding (JMC, GM and TB); JMC is also grateful for a Junior Research Fellowship funded by St Catharine's College, Cambridge.

References

Acet M, Brennan T, Cankurtaran M, Saunders G A and Zähres H 1998 *Phil. Mag.* B **77** 1633

Anderson R, Brennan T, Cole J M, Mountjoy G, Pickup D M, Newport R J and Saunders G A 1999 *J. Mater. Res.* **14** 4706

Binsted N, Campbell J W, Gurman S J and Stephenson P C 1991 CCLRC Daresbury Laboratory EXBACK and EXCURV92 programs

Borowski M, Bowron D T and De Panfilis S 1999 *J. Synchrotron Radiat.* **6** 179

Bowron D T, Bushnell-Wye G, Newport R J, Rainford B D and Saunders G A 1996a *J. Phys.: Condens. Matter* **8** 3337

Bowron D T, Newport R J, Rainford B D, Saunders G A and Senin H B 1995 *Phys. Rev.* B **51** 5739

Bowron D T, Saunders G A, Newport R J, Rainford B D and Senin H B 1996a *Phys. Rev.* B **53** 5268

Braglia M, Bruschi C, Dai G, Kraus J, Mosso S, Meneghini C, Balerna A, Boscherini F, Pascarelli S and Lamberti C 1999a *J. Non-Cryst. Solids* **257** 83

Braglia M, Dai G, Mosso S, Pascarelli S, Boschirini F, Balerna A and Lamberti C 1999b *J. Appl. Phys.* **85** 7987

Braglia M, Dai G, Mosso S, Pascarelli S, Boscherini F and Lamberti C 1998 *J. Appl. Phys.* **83** 5065

Brennan T, Knight J K and Saunders G A 1999 *Phys. Chem. Glasses* **40** 111

Carini G, D'Angelo G, Tripodo G, Fontana A, Rossi F and Saunders G A 1997 *Europhys. Lett.* **40** 435

Cole J M, Lees M R, Howard J A K, Newport R J, Saunders G A and Schoenherr E 2000 *J. Solid State Chem.* **150** 377

Cole J M, van Eck E R H, Mountjoy G, Newport R J, Brennan T and Saunders G A 1999 *J. Phys.: Condens. Matter* **11** 9165

Cole J M, van Eck E R H, Mountjoy G, Anderson R, Brennan T, Bushnell-Wye G, Newport R J and Saunders G A 2001 *J. Phys.: Condens. Matter* **13** 4105

Danielmayer H G, Jeser J P, Schoenherr E and Stetter W 1974 *J. Cryst. Growth* **22** 298

Di Cicco A 1995 *Physica* B **208/209** 125
——1997 *J. Physique Coll.* IV C2 171
Farok H M, Saunders G A, Poon W and Vass H 1992 *J. Non-Cryst. Solids* **142** 175
Filipponi A 1991 *J. Phys.: Condens. Matter* **3** 6489
Filipponi A and Di Cicco A 1995 *Phys. Rev.* B **52** 15 135
Filipponi A, Di Cicco A and Natoli C R 1995 *Phys. Rev.* B **52** 15 122
Filipponi A, Di Cicco A, Tyson T A and Natoli C R 1992 *GNXAS Package Documentation* (Camerino University Press)
Gurman S J, Binsted N and Ross I 1984 *J. Phys. C: Solid State Phys.* **17** 143
——1986 *J. Phys. C: Solid State Phys.* **19** 1845
Hong H Y-P 1974 *Acta Crystallogr.* B **30** 468
Hoppe U, Kranold R, Stachel D, Barz A and Hannon A C 1998 *J. Non-Cryst. Solids* **232–234** 44
Jia Y Q 1991 *J. Solid State Chem.* **95** 184
Kasatani H, Ohmura M, Yokoyama K, Kobayashi K, Nishihata Y, Yagi K and Terauchi H 1999 *Japan. J. Appl. Phys.* **38** 433
Kuzmin A and Grisenti R 1994 *Phil. Mag.* B **70** 1161
Li G G, Bridges F and Booth C H 1995 *Phys. Rev.* B **52** 6332
Lipinska-Kalita K E, Fontana A, Leonardi A, Carini G, D'Angelo G, Tripodo G and Saunders G A 1995 *Phil. Mag.* **71** 571
Lee P A and Pendry J B 1975 *Phys. Rev.* B **11** 2795
Loeffen P W, Pettifer R F, Müllender S, van Veenendaal M A, Röhler J and Sivia D S 1996 *Phys. Rev.* B **54** 14 877
Mierzejewski A, Saunders G A, Sidek H A A and Bridge B 1988 *J. Non-Cryst. Solids* **104** 323
Mountjoy G, Cole J M, Brennan T, Newport R J, Saunders G A and Wallidge G W 2001 *J. Non Cryst. Solids* **279** 20
Mustre de Leon J, Rehr J J, Zabinsky S I and Albers R C 1991 *Phys. Rev.* B **44** 4146
Nishihata Y, Kamishima O, Kubozono Y, Maeda H and Emura S 1998 *J. Synchrotron Radiat.* **5** 1007
Pettifer R P and Cox A D 1982 *EXAFS and Near Edge Structure* ed A Bianconi, L Incoccia and S Stipich (Berlin: Springer) p 66
Sayers D E, Stern E A and Lytle F W 1971 *Phys. Rev. Lett.* **27** 1204
Shannon C E and Weaver W 1963 *The Mathematical Theory of Communication* (Urbana, IL: University of Illinois Press) p 100
Shannon R D 1976 *Acta Crystallogr.* A **32** 751
Stern E A and Kim K 1981 *Phys. Rev.* B **23** 3781
Young J F 1971 *Information Theory* (London: Butterworth) p 87
Zabinsky S I, Rehr J J, Ankudinov A, Alberts R C and Eller M J 1995 *Phys. Rev.* B **52** 2995